Molecular beam epitaxy growth of $Zn_xCd_{(1-x)}Se/Zn_{x'}Cd_{y'}Mg_{(1-x'-y')}Se$-InP quantum cascade structures

W.O. Charles [a,*], K.J. Franz [b], A. Shen [a], Q. Zhang [c], Y. Gong [d], B. Li [a], C. Gmachl [b], M.C. Tamargo [e]

[a] Department of Electrical Engineering, The City College of CUNY, Marshak Science Building J1121, Convent Avenue and 138th Street, New York, NY 10031, USA
[b] Department of Electrical Engineering, Princeton University, Princeton, NJ 08544, USA
[c] Department of Physics, The City College and Graduate Center of CUNY, New York, NY 10031, USA
[d] Department of Applied Physics and Mathematics, Columbia University, New York, NY 10027, USA
[e] Department of Chemistry, The City College and Graduate Center of CUNY, New York, NY 10031, USA

ARTICLE INFO

ABSTRACT

We report growth by molecular beam epitaxy of a $Zn_xCd_{(1-x)}Se/Zn_{x'}Cd_{y'}Mg_{(1-x'-y')}Se$ quantum cascade (QC) structure that was designed for electroluminescence (EL) at ~4.5 μm. The QC active region is comprised of a two-well asymmetric coupled quantum well (ACQW) structure, which was thoroughly investigated to establish the growth conditions for the QC structure. After growth of several ACQW test samples, the conditions for growth were optimized for the QC structure. In-situ RHEED, photoluminescence (PL), high-resolution X-ray diffraction (HR-XRD) and Fourier transform infrared (FTIR) spectroscopy results were used for characterization. The QC structure grown under these conditions exhibited EL at 4.8 μm, in excellent agreement with the design value.

© 2008 Elsevier B.V. All rights reserved.

1. Introduction

Recently, there has been great success in the production of mid-infrared quantum cascade (QC) lasers using the InGaAs/InAlAs on InP materials system that emit light in the 4–24 μm region [1–4]. Within this wavelength range, the technology has progressed to the point where QC lasers are now finding commercial applications. These lasers can be made to operate in the absence of cryogenic cooling, allowing them to be part of very portable gas-sensing instruments and infrared transmitters. Due to the high output power, tunability, and narrow linewidth of their emission, these devices are ideally suited for commercial applications in the areas of chemical spectroscopy and high-speed free-space telecommunication [5–7]. However, research for QC structures operating below 4 μm using InGaAs/InAlAs has not

had similar success because of the limited conduction band offset (CBO) of this material system [8,9]. This limitation has led to the exploration of alternative materials.

With CBOs of 2.1 and 1.6 eV, several authors have reported QCL emission as low as 2.75 μm using InAs/AlSb on InAs and InGaAs/AlAsSb on InP [8–10]. However, the performance of the Sb-based devices is still not comparable to their InGaAs/InAlAs counterparts at longer wavelengths. This is in part due to the limitation of the effective CBO of InAs/AlSb and InGaAs/AlAsSb to about 0.8 and 0.5 eV, respectively, due to inter-valley electron scattering [10,11]. Also, in the case of the InAs/AlSb device, low optical confinement factor (~52%) and growth-related issues may be some of the reasons for the limited performance [10,12].

We have recently reported the observation of electroluminescence emission in QC emitter structures made from the II–VI $Zn_xCd_{(1-x)}Se/Zn_{x'}Cd_{y'}Mg_{(1-x'-y')}Se$ grown lattice-matched on InP substrates [13]. This is the first report of QC electroluminescence from a non-III–V semiconductor. With an absence of inter-valley electron scattering and an effective CBO of 1.12 eV [14], this materials system is very promising for producing

* Corresponding author. Tel.: +1 212 650 6147; fax: +1 212 650 6107.
E-mail address: wocharles99@aol.com (W.O. Charles).

high-performance QC lasers emitting below 4 μm. In this paper, we report the detailed growth process by molecular beam epitaxy (MBE) of the II–VI materials and multi-layered structures. We show that the optimized growth sequence leads to high crystalline quality and the precise composition and thickness control (afforded by MBE) as needed for these highly engineered and complex multi-layered device structures.

2. Experiment

In order to investigate the $Zn_xCd_{(1−x)}Se/Zn_{x'}Cd_{y'}Mg_{(1−x'−y')}$ Se-InP suitability for QCL fabrication, a QC emitter structure consisting of several hundred layers of alternating $Zn_xCd_{(1−x)}Se$ and $Zn_{x'}Cd_{y'}Mg_{(1−x'−y')}Se$ with precise thicknesses and compositions was designed to emit light at a wavelength of 4.5 μm. Although the CBO will allow emission at shorter wavelengths, in order to improve our chances of demonstrating the device operation we chose to design it at this slightly longer wavelength. Several calibration samples were grown to determine the growth conditions for producing lattice-matched $Zn_xCd_{(1−x)}Se$ and $Zn_{x'}Cd_{y'}Mg_{(1−x'−y')}Se$ layers and quantum wells with a CBO of ∼0.80 eV. Calibration layers doped n-type with $ZnCl_2$ were also grown and Hall effects measurements were made to determine the carrier concentrations in the III–V and II–VI epilayers that are needed for the device structures.

Based on these calibration runs, the material composition for the II–VI epilayers was selected to be $Zn_{0.43}Cd_{0.57}Se$ and $Zn_{0.20}Cd_{0.19}Mg_{0.61}Se$. These compositions produce ternary and quaternary layers lattice-matched to InP with bandgaps of 2.08 and 3.03 eV at 300 K, respectively, and are expected to have a CBO of 0.78 eV [15]. The QC emitter was designed using a program that utilizes the envelope function approximation assuming an electron effective mass of $m_0 \times 0.128$ and $m_0 \times 0.181$ (where m_0 is the free electron mass) for $Zn_{0.43}Cd_{0.57}Se$ and $Zn_{0.20}Cd_{0.19}Mg_{0.61}Se$, respectively [16]. The simulation results showing the squared moduli of the wave functions in the conduction band is displayed in Fig. 1. The proposed structure is composed of 20–30 repeats of asymmetric coupled quantum well (ACQW) active regions with alternating (multi-layer) injector regions. One period of the designed structure starting from the injection barrier is made up of the following layers in angstroms: **30**/34/**10**/28/**20**/24/**10**/22/**12**/20/**16**/20/**18**/18/**18**/18/**20**/16/**20**/16/**20**/14/**22**/14/**24**/12/**26**/12 with the $Zn_{0.20}Cd_{0.19}Mg_{0.61}Se$ barrier indicated in bold and

the Cl-doped layers underlined. The ACQW layers are shown in italics.

In order to establish the accurate growth parameters that would lead to the growth of this complex multi-layered structure, another set of calibration samples composed of several repeats of the ACQW layers separated by simple quaternary barrier layers, rather than the multi-layered injector regions, were grown. The alternating ACQWs and quaternary barrier layers were repeated 25 times and the wells were doped with chlorine ($n \sim 4 \times 10^{18}$ cm^{-3}) in order to observe inter-sub-band (ISB) absorption through multi-pass transmission experiments using Fourier transform IR (FTIR) spectroscopy [17]. Prior to the growth of the ACQW test structures, individual layers were grown to determine the exact growth rate and composition of the well and barrier materials used. In some of the samples, RHEED intensity oscillation measurements were made to accurately determine the growth rates.

The structures were grown on (0 0 1) InP substrates by solid source MBE in a Riber 2300P dual chamber system that consists of a growth chamber dedicated to III–V materials and another dedicated to II–VI materials. The two chambers are interconnected via ultra-high vacuum modules that allow the transfer of samples between them in vacuum. Before the growth of the II–VI layers, the InP substrate is heated in the III–V chamber under an arsenic overpressure until desorption of the oxide surface layer is achieved. The oxide desorption is assured by observing the transition from a (2×4) As-stabilized InP surface to the (4×2) In-stabilized InP surface. On observing this transition, the substrate temperature is rapidly lowered by 30 °C before commencing growth of a lattice-matched $In_{0.53}Ga_{0.47}As$ buffer layer. The InGaAs buffer with a growth rate of 1 μm/h is grown for 15 min under As-rich growth conditions at a substrate temperature that is 30° below the oxide layer desorption temperature. This 0.25 μm InGaAs buffer layer is grown to ensure that a smooth III–V surface with group-V termination is present for the initiation of the II–VI layer growth.

A sequence of steps has previously been developed to initiate ZnCdSe growth on an InGaAs surface [18]. Upon completion of the InGaAs layer growth, the sample is transferred to the II–VI chamber where the As-terminated InGaAs surface is exposed to a zinc flux for 40 s at a temperature of 200 °C (Zn-irradiation). The Zn-irradiation step is performed to suppress the formation of In_2Se_3 and Ga_2Se_3 compounds at the III–V/II–VI interface. The presence of these selenium compounds must be minimized to prevent the formation of defects such as stacking faults that are known to degrade the material. This is followed by the growth of a low-temperature (200 °C) $Zn_{0.43}Cd_{0.57}Se$ buffer layer 90 s (∼90 Å) to promote two-dimensional nucleation. It was previously shown that this sequence of steps, including the low-temperature $Zn_{0.43}Cd_{0.57}Se$ interfacial layer growth results in high-quality epitaxy and reduces the defect densities to ∼10^4 cm^{-3} [19]. After the low-temperature layer, the growth is interrupted and the substrate temperature is raised and stabilized at 300 °C under a selenium flux before resuming the growth of the II–VI structure. The growth rates of ZnCdSe and ZnCdMgSe were typically 0.30 and 0.85 μm/h, respectively, and the Se/group-II flux ratio was maintained at above 4, to ensure Se-stabilized growth conditions. Measurement of the RHEED intensity oscillations was typically done after the growth interruption, at the initiation of the growth at 300 °C. The RHEED intensity oscillation traces, shown in Fig. 2a and b, indicate a clear layer-by-layer growth mechanism during the growth of these materials, and enable us to establish the growth rates with high accuracy. After growth, the ACQW structure samples were analyzed using PL, HR-XRD, and FTIR spectroscopy.
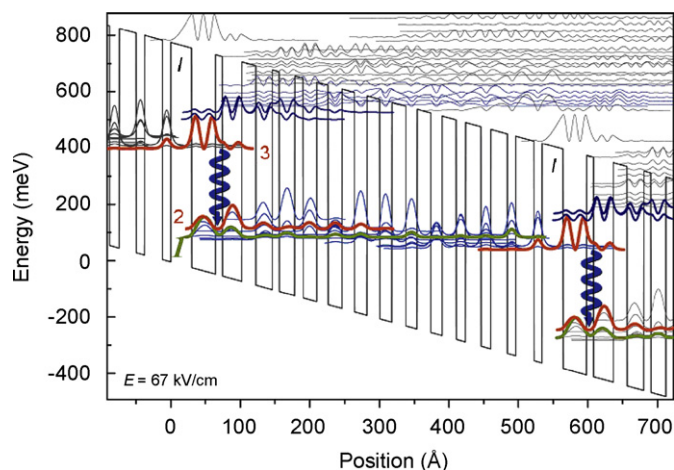

Fig. 1. Simulation of the band structure of the QC emitter structure showing the modulus square of the wave function within the active/injector regions. *'I'* denotes the injection barrier at the start of one active/injector period [13].
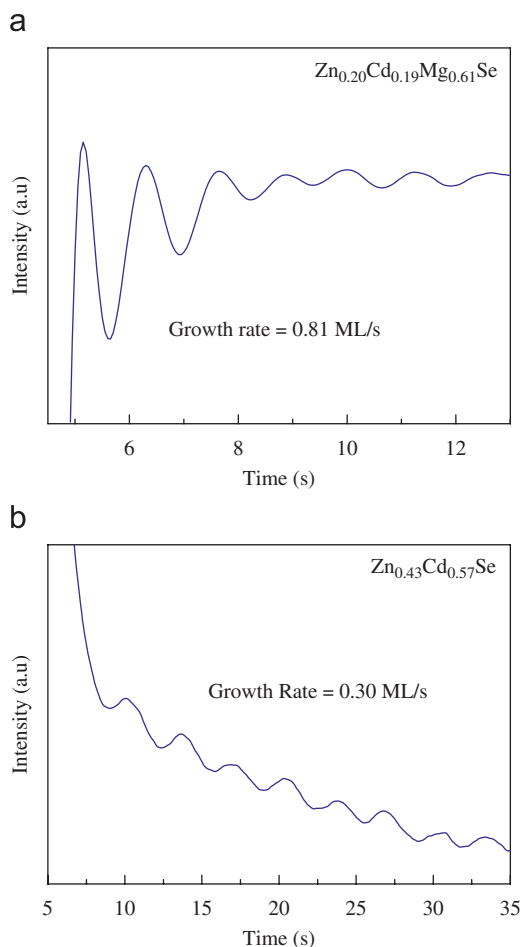
a

b

Fig. 2. Traces of the RHEED intensity oscillations measured during growth of (a) $Zn_{0.20}Cd_{0.19}Mg_{0.61}Se$ and (b) $Zn_{0.43}Cd_{0.57}Se$ calibration samples.

3. Results/discussion

The room temperature FTIR absorption for the first ACQW structure grown is shown in Fig. 3. The two absorption peaks seen at 0.240 and 0.301 eV were assigned to the e_2-e_3 and e_1-e_3 transitions. Simulations based on the envelope function approximation, predict e_2-e_3 and e_1-e_3 absorption at 0.266 and 0.313 eV, respectively. Furthermore, a separation of e_2-e_1 of 0.061 eV is deduced from the two FTIR peaks, while the predicted value based the simulation was 0.047 eV [17]. The combination of these energy discrepancies is consistent with the ACQW barrier being slightly thinner than intended. At this point, the growth was re-calibrated and a second ACQW structure was grown and characterized. For the re-calibration, we incorporated the use of RHEED intensity oscillations to improve the accuracy of the growth rates.

The layer sequence in angstroms for one period of the second ACQW structure is as follows; **110**/34/**10**/28, where the chlorine-doped well layers are underlined and the barrier (quaternary) layers are in bold. The nominal (design) thickness of one period of the structure is 182 Å. Using an average satellite spacing of $\delta 2\theta = 0.59°$ obtained from the HR-XRD plot shown in Fig. 4, the grown period thickness was calculated to be 176 Å, indicating very good control of the well/barrier thickness (∼3% difference). The inset in Fig. 4 shows an expanded view of the region near the zero-order peak. Clear interference fringes can be seen in the inset also indicating excellent material quality. This test sample was also investigated using PL and the results are shown in Fig. 5. The
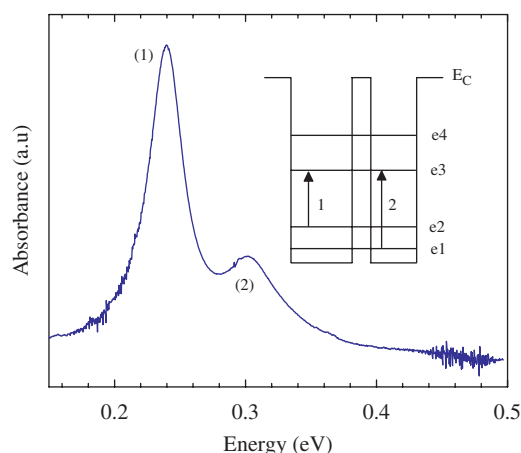

Fig. 3. FTIR spectrum for the first ACQW structure grown. The inset describes the energy-level distribution. Peaks (1) and (2) represents absorption e_1-e_3 (0.301 eV or $\lambda = 4.13\,\mu m$) and e_2-e_3 (0.240 eV or $\lambda = 5.18\,\mu m$) absorption, respectively. From these results the e_1-e_2 separation was calculated to be 0.061 eV.
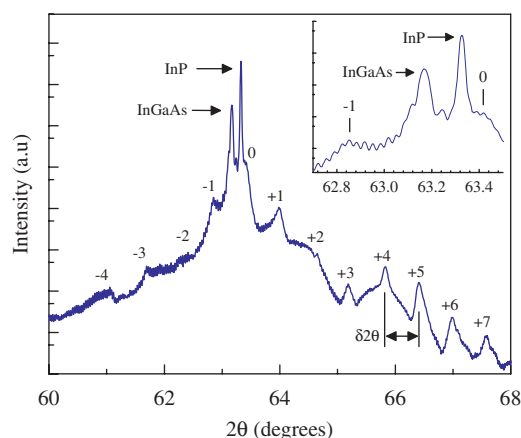

Fig. 4. HR-XRD spectra for the second ACQW structure plotted on a logarithmic scale. The inset is an expanded region around the zero-order peak showing the presence of thickness fringes, characteristic of very high-quality material.
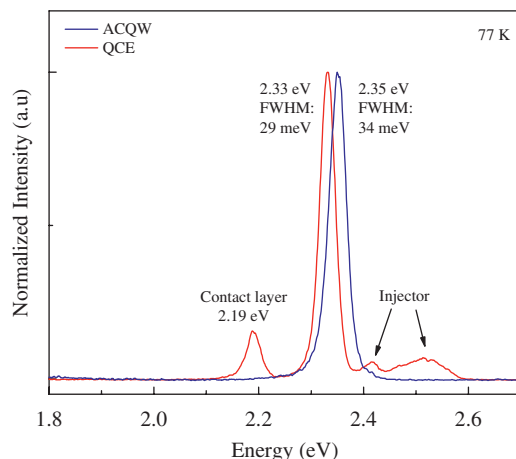

Fig. 5. PL spectra at 77 K for the second ACQW and the QC emitter structures.

linewidth of the PL at 77 K was 34 meV. This narrow linewidth and the absence of deep levels in the PL spectrum confirm that the material and the well/barrier interface quality are good.

The second ACQW structure was processed into a waveguide with 45° facets for use in FTIR spectroscopy. The infrared light
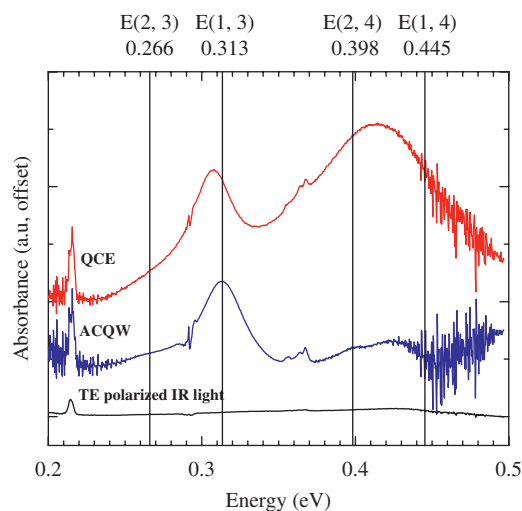
Fig. 6. FTIR absorption spectra for the second ACQW and the QC emitter structures at 300 K. The vertical lines represent the simulation results for the ACQW structure.
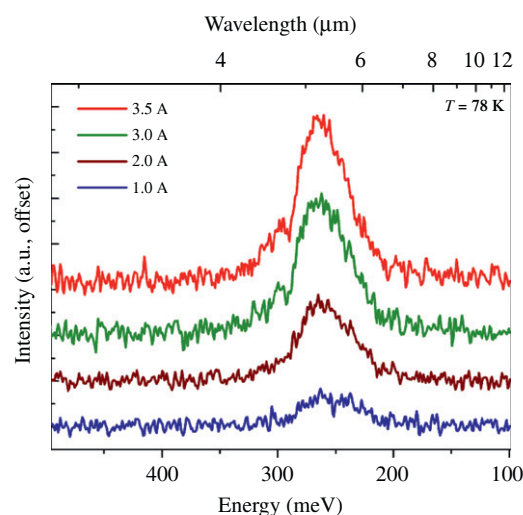

Fig. 7. EL spectra for the QC emitter for drive currents ranging from 1.0 to 3.5 A at 78 K. The emission peak is centered at 4.8 μm [13].

from the Nexus 670 FTIR spectrometer was allowed to pass through a polarizer, which was used to resolve the light into its TM and TE components. The light that passed through the polarizer was then focused onto a 45° facet of the sample using a ZnSe lens. After making several bounces through the waveguide the light that emerged through the second facet was collected and focused onto a liquid-nitrogen-cooled external mercury cadmium telluride (MCT) detector using another set of ZnSe lenses. The room temperature FTIR spectrum for the second ACQW structure is shown in Fig. 6. The vertical lines represent the values predicted by the simulation for this ACQW structure. One dominant absorption peak is seen, and it is assigned to the e_1–e_3 transition, which agrees very well with the simulation results. Figs. 5 and 6 also show, for comparison, the PL and FTIR absorption spectra for the QC structure that was grown according to these improved growth parameters [13]. The slight red shift in the QC structure's e_1–e_3 FTIR absorption energy relative to the same transition in the ACQW structure is consistent with a reduction in the energy-level spacing expected when the thick quaternary barrier in the ACQW structure is replaced with a digital superlattice injector in the QC emitter structure. We tentatively identify the broad, higher-energy absorption as originating from the e_2–e_4 and e_1–e_4 transitions present in the un-biased QC emitter structure. In addition to the dominant peak due to emission from the active region, the PL spectrum of the QC emitter exhibits emissions originating from the injector region and the contact layer. The presence of the superlattice injector regions in the QC structure is also responsible for the slight red shift of the dominant PL emission peak.

As previously reported, the QC samples were processed into QC emitters using photolithography with metal contacts added using electron beam metal deposition [13]. Electroluminescence (EL) from a 0.036 mm^2 QC emitter heat-sinked at 78–300 K was collected for drive currents ranging from 1.0 to 3.5 A using a FTIR spectrometer in step scan mode and a cooled MCT detector [13]. The QC emitter electroluminescence at 78 K, shown in Fig. 7, is centered at 4.8 μm, which is in excellent agreement with the design emission wavelength of 4.5 μm.

4. Conclusion

In conclusion, a $Zn_{0.43}Cd_{0.57}Se/Zn_{0.20}Cd_{0.19}Mg_{0.61}Se$-InP QC emitter was designed for emission at 4.5 μm. In order to establish the optimum growth parameters needed to achieve the appropriate energy-level distribution in the active region of the QC structure, two ACQW test samples were grown and investigated. PL and HR-XRD analysis of the test samples indicate that the multi-layers in this materials system can be grown with very high quality and control, comparable to that demonstrated in III–V QC structures. More specifically, the HR-XRD shows that the well/barrier layer thickness can be controlled to within 3% of the desired value. After careful calibration of the growth parameters, including the use of RHEED intensity oscillation measurements to accurately establish the ternary and quaternary layer growth rates, FTIR results for the second ACQW and QC emitter structures were compared with simulation results. The measured FTIR peaks are in good agreement with the values predicted by the simulation. A QC emitter sample grown with these optimized conditions was processed and investigated for electroluminescence. The measured emission wavelength of 4.8 μm also compares very well with the design value of 4.5 μm. These results demonstrate that the growth of $Zn_xCd_{(1-x)}Se/Zn_{x'}Cd_{y'}Mg_{(1-x'-y')}Se$ on InP substrates by molecular beam epitaxy can be accurately controlled to provide the stringent layer thickness, composition control, and excellent material quality that are needed for these complex multi-layered device structures.

References

[1] A. Lyakh, C. Pflugl, L. Diehl, Q.J. Wang, F. Capasso, X.J. Wang, J.Y. Fan, T. Tanbun-Ek, R. Maulini, A. Tsekoun, R. Go, C.N. Patel, Appl. Phys. Lett. 92 (2008) 111110.
[2] R. Colobelli, F. Capasso, C. Gmachl, A.L. Hutchinson, D.L. Sivco, A. Tredicucci, M.C. Wanke, A.M. Sergent, A.Y. Cho, Appl. Phys. Lett. 78 (2001) 2620.
[3] Z.J. Liu, D. Wasserman, S.S. Howard, C.F. Gmachl, X.J. Wang, T. Tanbun-Ek, L.W. Cheng, F.S. Choa, IEEE Photon. Tech. Lett. 18 (2006) 1347.
[4] S. Blaser, A. Bachle, S. Jochum, L. Hvozdara, G. Vandeputte, S. Brunner, S. Hansmann, A. Muller, J. Faist, Electron. Lett. 43 (2007) 1201.
[5] B.G. Lee, M.A. Belkin, R. Audet, J. MacArthur, L. Diehl, C. Pflugl, F. Capasso, Appl. Phys. Lett. 91 (2007) 231101.

[6] R. Martini, C. Bethea, F. Capasso, C. Gmachl, R. Paiella, E.A. Whittaker, H.Y. Hwang, D.L. Sivco, J.N. Baillargeon, A.Y. Cho, Electron. Lett. 38 (2002) 181.
[7] A. Kosterev, F. Tittel, IEEE J. Quant. Elect. 38 (2002) 582.
[8] J. Devenson, D. Barate, O. Cathabard, R. Teissier, A.N. Baranov, Appl. Phys. Lett. 89 (2006) 191115.
[9] D.G. Revin, J.W. Cockburn, Appl. Phys. Lett. 90 (2007) 021108.
[10] J. Devenson, O. Cathabard, R. Teissier, A.N. Baranov, Appl. Phys. Lett. 91 (2007) 251102.
[11] Q. Yang, C. Manz, W. Bronner, k. Kohler, J. Wagner, Appl. Phys. Lett. 88 (2006) 121127.
[12] X. Marcadet, C. Renard, M. Carras, M. Garcia, J. Massies, Appl. Phys. Lett. 91 (2007) 161104.
[13] K.J. Franz, W.O. Charles, A. Shen, A.J. Hoffman, M.C. Tamargo, C. Cmachl, Appl. Phys. Lett. 92 (2008) 121105.
[14] M. Sohel, M. Munoz, M.C. Tamargo, Appl. Phys. Lett. 85 (2004) 2794.
[15] M. Sohel, X. Zhou, H. Lu, M.N. Perez-Paz, M.C. Tamargo, M. Munoz, J. Vac. Sci. Technol. B 23 (2005) 1209.
[16] M. Munoz, H. Lu, X. Zhou, M.C. Tamargo, F.H. Pollak, Appl. Phys. Lett. 83 (2003) 1995.
[17] W.O. Charles, A. Shen, K.J. Franz, C. Gmachl, Q. Zhang, Y. Gong, G.F. Neumark, M.C. Tamargo, J. Vac. Sci. Technol. B 26 (2008) 1171.
[18] L. Zeng, S.P. Guo, Y.Y. Luo, W. Lin, M.C. Tamargo, H. Xing, G.S. Cargill III., J. Vac. Sci. Technol. B 17 (1999) 1255.
[19] L. Zeng, B.X. Yang, M.C. Tamargo, E. Snoeks, L. Zhao, Appl. Phys. Lett. 72 (1998) 1317.